Atomic scale insights into the first reaction stages prior to Al/CuO nanothermite ignition: influence of porosity

Hicham Jabraoui, Alain Esteve, Mirko Schoenitz, Edward L Dreizin, Carole Rossi

Atomic scale insights into the first reaction stages prior to Al/CuO nanothermite ignition: influence of porosity

Hicham Jabraoui, Alain Esteve, Mirko Schoenitz, Edward L Dreizin, Carole Rossi*

* E-mail: rossi@laas.fr

Abstract

This theoretical work aims to understand the influence of nanopores at CuO-Al nanothermite interfaces on the initial stage of thermite reaction. ReaxFF molecular dynamics simulations were run to investigate the chemical and structural evolution of the reacting interface between the fuel, Al, and oxidizer, CuO, between 400 and 900 K and considering interfaces with, and without a pore. Results show that the initial alumina layer becomes enriched with Al and grows primarily into the Al metal at higher temperatures. The modification of alumina is driven by simultaneous Al and O migration between metallic Al and the native amorphous Al_2O_3 layer. However, the presence of a pore affects significantly the growth kinetics and the composition of this alumina layer at temperatures exceeding 600 K, which impacts the initiation properties of the nanothermite. In the system without pore, where Al is in direct contact with CuO, a ternary aluminate layer, a mixture of Al, O and Cu, is formed at 800 K which slows Al and O diffusion, thus compromising the nanothermite reactivity in fully-dense Al/CuO composites. Conversely, the presence of a pore between Al and CuO promotes Al-enrichment of the alumina layer above 600 K. At that temperature, any free oxygen molecules in the pore become attached to the reactive alumina surface resulting in a rapid oxygen pressure drop in the pore. This is expected to accelerate the reduction of the adjacent CuO as observed in experiments with Al/CuO composites with porosity at the CuO-Al interfaces.

KEYWORDS: nanothermites, nanoenergetics, heterogeneous kinetic, reactive interface, nanocomposite, molecular dynamic, ReaxFF.

1. Introduction

Nanothermites are mixtures of nanosized reactants which are stable under moderate conditions and capable of interacting with each other with the release of large amounts of chemical energy after activation by a triggering stimulus (thermal, mechanical, or electrical). Much research in nanothermites have focused on Al based systems such as Al/Fe_2O_3, Al/MoO_3, Al/CuO, and Al/Bi_2O_3 due to their high energy density [1,2], and combustion performance tunability [3,4]. Al-based nanothermites have found applications for joining or welding [5,6,], tunable generators of biocidal-agents [7,8], actuation in initiators/detonators [9–11] and in single-use miniaturized microelectromechanical systems [12–15]. A key parameter to high reactivity in nanothermites is intimate interfacial contact between fuel (Al) and oxidizer. That is why various preparation methods have been employed to combine aluminum fuel and oxidizer together in close proximity, including sputter deposition [16–18], arrested milling methods [19], electrospray [20], sol−gel processing [21], and self-assembly [22–25]. Interestingly, in Al/CuO fully-dense materials such as composites prepared by arrested reactive milling (ARM)[26] and reactive multilayers [3], the exothermic redox reaction is restricted to condensed phase reactions at the CuO-Al interface, where an amorphous product Al_2O_3 layer grows [27–29] and the ignition temperature is reduced compared to other types of thermites to ~850 K. [30,31] Recent studies also showed that the ignition temperature can be further decreased by adding micro or nano voids within the interfacial layer, which was unexpected. Mursalat et al.,[32] observed that modifying the milling process parameters, i.e., adding a premilling step for Al

powders using acetonitrile as a process control agent produces nano-voids in the thermite, resulting in lowering the ignition temperature down to ~650 K [32,33] and accelerating the reaction. Wu et al., [34] also showed that incorporation of micro-sized pores into Al/CuO reactive multilayers decreases the ignition threshold around the pores and provokes the acceleration of their burn rate (×18% for 20% void loading). The authors concluded that voids or pores in the CuO-Al interface may modify the low-temperature chemical reaction sequence: instead of being driven by purely condensed phase diffusion over the CuO-Al interface, when pores are incorporated, gaseous O_2 is released by CuO in contact with the pores at very low temperatures. This oxygen can diffuse into solid Al and Al_2O_3, leading to low ignition temperature (650 - 670 K). Two possible ignition pathways in Al/CuO nanolaminates have been also observed by time-of-flight mass spectrometer in [35]: in nanolaminates with 2 to 6 bilayers, gaseous O_2 is released prior to the ignition (spark) leading to a low ignition temperature (670 K) and enhanced overall reactivity compared to samples with 6 and more bilayers where initiation is controlled by condensed phase reactions (no gaseous O_2 signal is seen prior to the ignition). Those experimental findings point to the complexity of mechanisms governing the Al/CuO reactivity and raise an important question about the role the porosity at the CuO-Al interfaces might be playing to affect both the ignition and combustion in these composites. Creating controlled nanopores at the CuO-Al interfaces and probing the chemical evolution of the pores' surroundings at the nanoscale over a very short time to study the initial reaction stages experimentally is not yet possible. Addressing this issue theoretically using molecular dynamics (MD) is the most direct way to provide better understanding [36–38]. Only a few theoretical efforts [27–29,39] attempted to describe the early stage of reactions of Al with CuO using density functional theory (DFT) or *ab initio* molecular dynamics. They describe the Al/CuO reactivity upon annealing but over very short duration (20 ps) and in small systems (100s atoms), which are not representative of

experimental conditions. It was concluded that the increase in the rates of both Al oxidation and the migration of Cu atoms in aluminum oxide occur at high temperatures (2000 K and 3000 K). The theoretical studies reported so far have not been able to investigate reactions at low temperatures, i.e., reactions leading to ignition. Such low-temperature reactions may be of critical importance as altering the structure of the reactive interfaces, and further affect the reactivity and combustion in fully-dense Al/CuO composites.

This study aims to understand how the structural features of the interface may affect the ignition characteristics. To this end, the evolution of the characteristics of the interface between Al (and associated Al_2O_3 surface layer) and CuO in terms of chemical composition, structure, and growth rate are investigated theoretically using reactive force field (ReaxFF) MD simulations and varying two parameters: temperature from 400 – 900 K, and the interface structure: interfaces with or without pore (1 nm spacing between Al_2O_3 and CuO surfaces containing free oxygen molecules). Upon heating, simulations show the growth of an Al-rich alumina region in both porous and dense systems in place of the initial amorphous alumina barrier layer. Major differences between the porous and dense systems emerge when the temperature exceeds 600 K. The direct contact between the Al_2O_3 and CuO leads to the formation of a ternary aluminate phase made of a mixture of Al, O and Cu atoms, which impedes the diffusion-driven reaction between Al and O, thus reducing the material reactivity. No ternary phase forms when CuO is separated from the alumina layer by a pore. The diffusion of Al and O species through the growing alumina is activated at 800 K in the presence of the ternary aluminate phase as compared to 600 K, for the case with a pore at the interface. As a direct consequence of the early enrichment of the alumina layer with Al, molecules of oxygen trapped in the pore are adsorbed and chemically incorporated into the alumina layer at 600 K, explaining the small exotherm at 600 K found on differential scanning calorimetric (DSC) traces of Al/CuO dense composites containing nanopores.

Noteworthy the pore O_2 pressure drop may trigger the decomposition of the adjacent CuO surface [52], thus supporting the presence of copper-rich nanodots (local reduction of CuO) observed in the partially reacted composites with voids at the interfaces [32]. Not only does this study bring consistent understanding of the Al/CuO pre-ignition mechanisms in porous versus fully-dense composites, but it also explains the decrease in the ignition temperature and increased reactivity experimentally observed for layered or milled Al/CuO composites containing nanopores.

2. Computational details

Using LAMMPS packages[40], MD simulations of atomic scale interactions at the CuO-Al interfaces were performed using periodic boundary conditions. The Nosé-Hoover thermostat and barostat served respectively to maintain the temperature in the canonical NVT ensemble, and the pressure in the isothermal–isobaric NPT ensemble. The ReaxFF force field parameters used in this study were developed by Psofogiannakis et al. [41]

The CuO material was built considering a cubic unit-cell with lattice parameters a = b = c = 4.23 Å and $\alpha = \beta = \gamma = 90°$ as described in ref [42], and replicating it in the three spatial directions (*x*, *y* and *z*) forming a supercell containing 640 O atoms and 640 Cu atoms. First, the CuO atoms in the supercell were allowed to relax at 300 K in the NPT ensemble over 0.1 ns. Then, an additional 0.1 ns relaxation of both the atomic positions and volume was performed for the supercell using a ReaxFF MD simulation at 300 K in the NVT ensemble. As a result, two 23.46 Å × 23.46 Å *x*,*y* surfaces cleaved normal to the [001] *z* direction formed, one O-rich surface that was chosen to be in contact with either the pore or the alumina layer, and one Cu-rich surface, which was frozen to mimic the CuO bulk material. This slab underwent a final relaxation step at 300 K over 0.1 ns in the NVT ensemble. Note that the *x*,*y* supercell dimension that used for the CuO-Al interface with a pore is calibrated

here on the basis of CuO rather than Al due to the CuO stability that necessitates finer tuning of cell dimensions.

To build the 2-3 nm thick native amorphous alumina coating any pure Al surface in contact with air [43], namely *am*Al_2O_3, we used non-reactive force field MD simulations adapted to both Born-Meyer-Higgins's potential formulation and long-range Coulomb interactions. We used the Ewald summation with a cutoff of 12.0 Å for the real part and a relative error in forces < 10^{-6}, while the short-range cutoff was set to 8.0 Å [44]. Fitting the *x*,*y* CuO slab dimension, a random structure of 1500 atoms (600 Al and 900 O) was first equilibrated at 4000 K for 1 ns to reach its liquid equilibrium state in the NVT ensemble. It was then quenched to 300 K at 10 $K \cdot ps^{-1}$ to reach the vitreous state in the NPT ensemble using an integration time step of 0.1 fs. The results are illustrated in **Figure 1a**. More details on this methodology are documented in refs [45–49]. Two *am*Al_2O_3 surfaces were generated by adding two vacuum slabs along *z* in either part of the *am*Al_2O_3 slab (**Figure 1b**). Finally, this *am*Al_2O_3 surface was annealed again at 300 K for 1 ns in the NVT ensemble with the same ReaxFF potential parameters[41]. Then, to build the Al-*am*Al_2O_3 interface, a pure Al slab containing 1008 atoms (in a face-centered cubic crystal structure) and cleaved normal to the [001] direction was connected to the as prepared *am*Al_2O_3 slab. Further chemical stabilization of this interface was realized through annealing in the NVT ensemble at 200 K over 1 ns.

Then, from these two elementary structures, Al/*am*Al_2O_3 and CuO, we derived two model systems: the dense and the porous system. The dense system was built by placing the Al/*am*Al_2O_3 slab in direct contact to the CuO slab whereas, in the porous system, Al/*am*Al_2O_3 and CuO slabs were separated by a vacuum space, the nanopore being 23.46 Å × 23.46 Å × 10 Å in dimension. We randomly introduced 13 O_2 molecules in the pore, equivalent to the saturated vapor pressure (5080 kPa). The final size of the supercell is of 23.46 Å × 23.46 Å × 110 Å and 23.46 Å × 23.46 Å × 120 Å, for dense and porous systems, respectively (**Figure**

1). As a final stage both systems underwent a relaxation step at 200 K over 1 ns to chemically stabilize all surfaces, including the *am*Al_2O_3/CuO interface. All annealing simulations were performed in the NVT ensemble and the time step is 1 fs. The top and bottom surface layers in the supercell were kept frozen during the entire simulation.

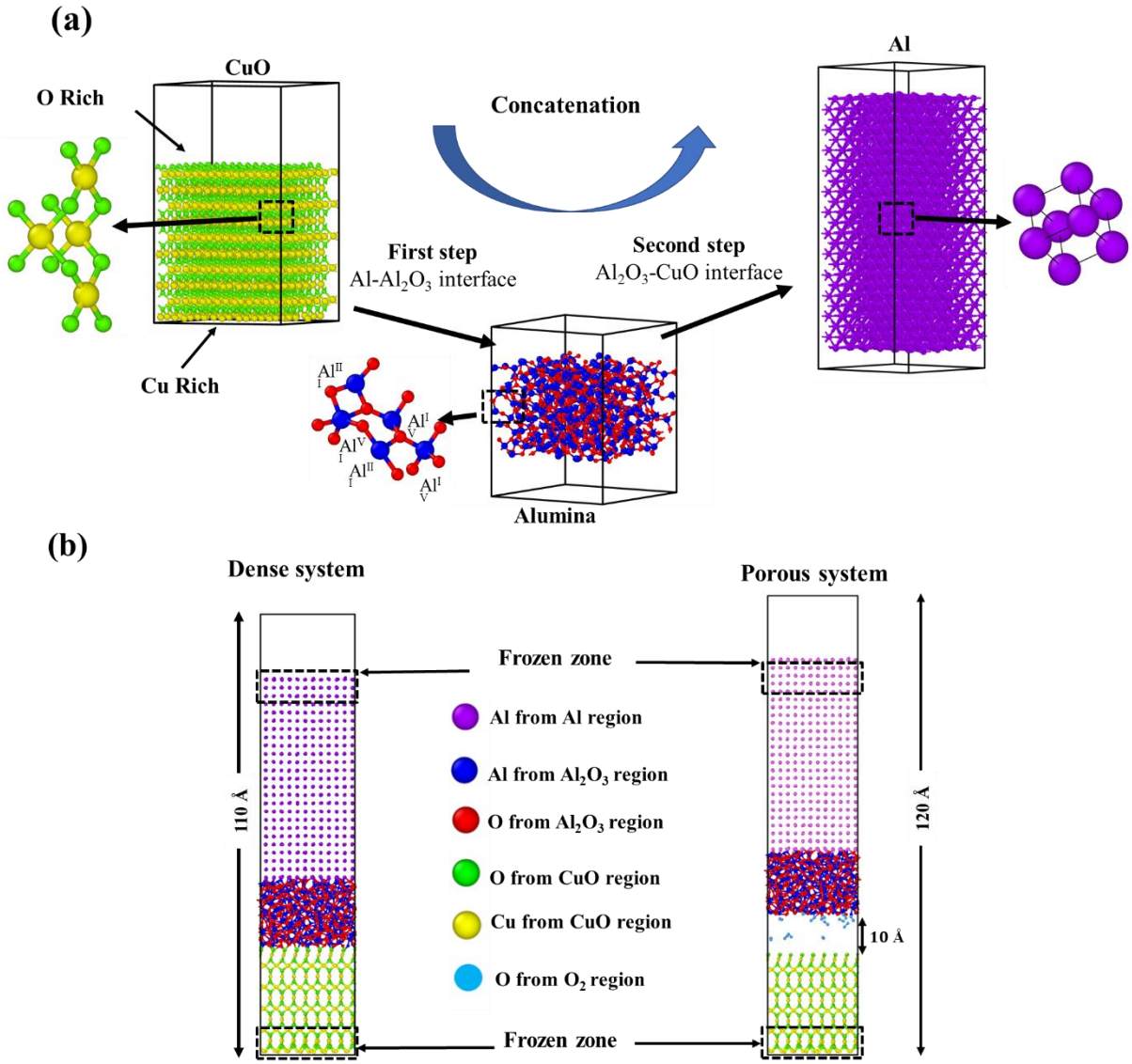

Figure 1. Schematic 2D views representing (a) the different steps of the model-system construction, and, (b) final structures of each model-system (dense and porous one).

3. Results and discussions

3.1. Effect of pore on evolution of the Al/CuO interface

The porous and fully-dense structures were heated up from 200 K to targeted temperatures, e.g., 400, 500, 600, 700, 800 and 900 K using a heating rate of 10^{13} K·s^{-1}, followed by a plateau of 5 ns. This duration was chosen because in all cases, the system reached a stationary state after ~3 ns, as shown in supporting information file **Figure S1**. A 10^{13} K.s^{-1} heating rate is imposed as an atomic motion damping procedure calibrated so that to avoid undesirable thermal shock at the very first stage of the simulations, leading to biased bond breaking. The structural and chemical composition evolution of the initial *am*Al_2O_3 region upon annealing are characterized for both systems.

Figure 2 gives side view snapshots of the annealed dense and porous systems at 500 K (b,f), 700 K (c,g) and 900 K (d,h) in comparison with the un-annealed structures (a,e). Other temperatures are provided in supporting information file **Figure S2**.

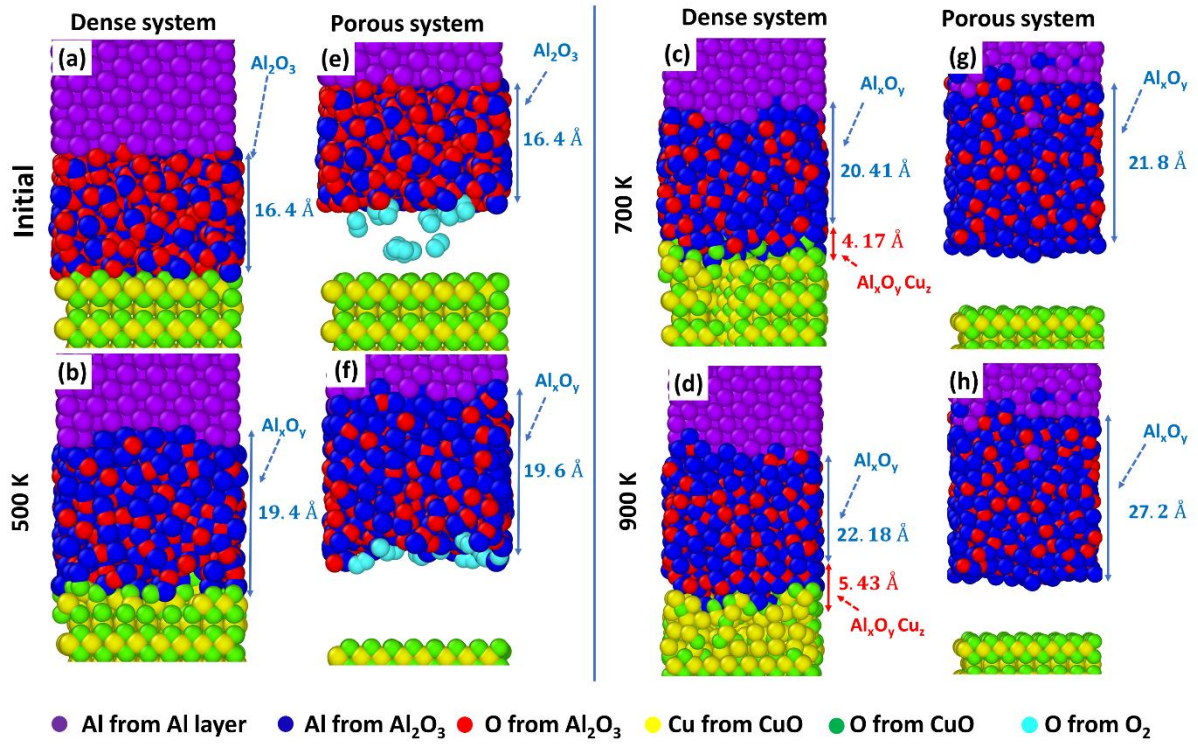

Figure 2. Two-dimensional views of initial (un-annealed) and final (post-annealed) structures at different selected temperatures (500, 700 and 900 K); Images a-d correspond

to the dense system and images e-h to the porous system.

First, we observe that in both porous and dense systems, the alumina layer, initially *am*Al_2O_3, thickens and converts into a non-stoichiometric $Al_{2+x}O_3$ upon annealing. $Al_{2+x}O_3$, labelled Al_xO_y in the rest of the paper, grows into the Al region, accompanied by a modification of its atomic composition, resulting from the migration of aluminum atoms from the Al region into the alumina interface and counter migration of O from the alumina towards the Al region.

Figure 3a-b and **Figure 3c-d** respectively give the depth of penetration of aluminum atoms through the alumina (ΔZ) and the quantity of aluminum atoms that penetrated into alumina from the metal (as the percentage of the overall additional Al) for both systems and at all annealing temperatures. The reference to calculate ΔZ is taken at the initial *am*Al_2O_3 surface (surface in contact with the pore or the CuO top surface). Below 600 K, there is no significant difference in the Al penetration behavior between the two systems, neither in the penetration depth of Al atoms nor in the quantity of metallic Al which penetrated into the alumina. However, at 600 K, the free-molecular oxygen species trapped in the pore are adsorbed at the Al_xO_y surface and start dissociating, giving a total of 12 atoms (out of 26) already fully incorporated into the Al_xO_y subsurface. At 600 K, in the dense system, only 9 oxygen atoms are predicted to transfer from the CuO to the Al_xO_y layer, pointing to the easier grabbing of the chemisorbed oxygen atoms, rather than rearranging the stable Al_xO_y-CuO interface.

Above 600 K, the evolution towards a more reactive alumina layer becomes substantially different between the two systems. First, the Al penetration is slowed down in the dense system, whereas it is promoted in the porous one. Indeed, at 700 K, one of the migrating Al atoms has reached the Al_xO_y-pore surface (violet Al atom, **Figure 3f**), whereas the deepest Al

atom in the dense system remains at 3 Å from the Al_xO_y–CuO interface (**Figure 3a-b**). A closer examination of the porous structure after 700 K annealing shows that the 26 oxygen atoms coming from the pore are randomly distributed in the Al_xO_y layer over an approximately 3 Å thickness. In contrast, in the dense system, oxygen atoms from CuO migrate in the Al_xO_y over only an approximately 1.6 Å thickness.

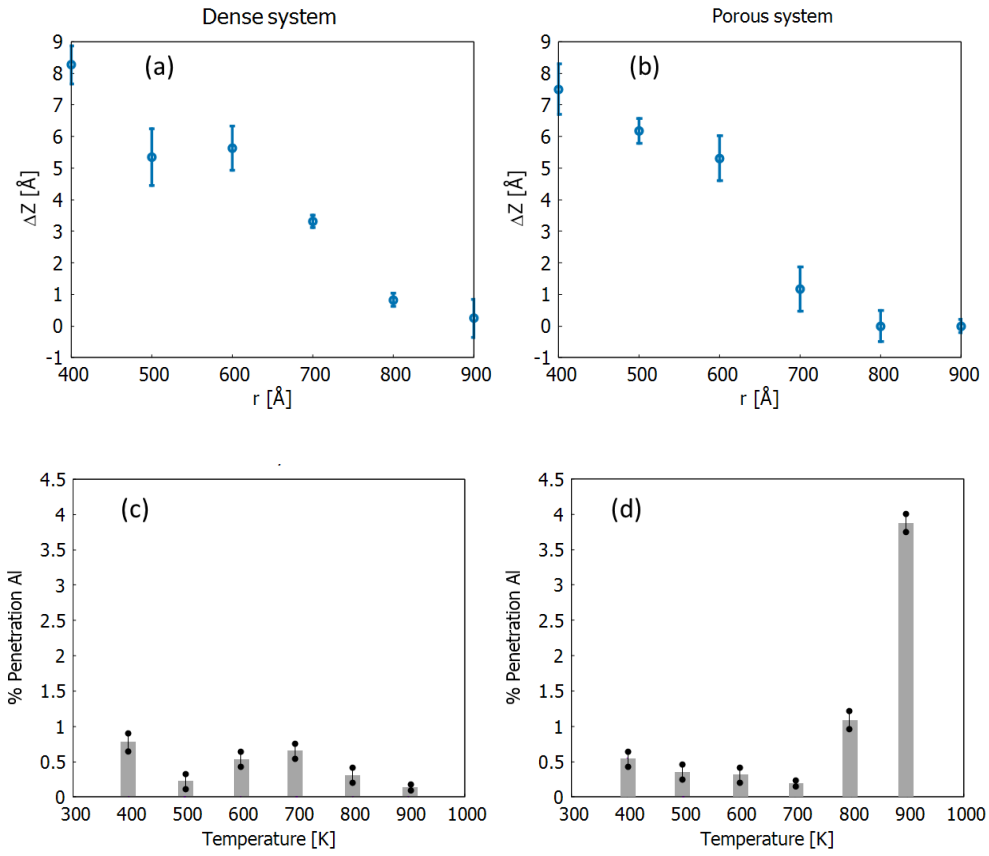

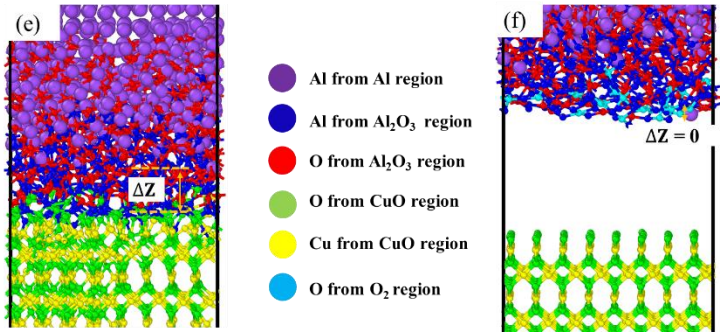

Figure 3. Penetration depth (ΔZ) into the native alumina region of Al atoms initially belonging to the metal upon annealing, with reference being made to the surface of Al_xO_y in contact with CuO or air for dense (a) or porous (b) systems, respectively. The amount of Al initially belonging to the metal that has reached the deepest penetration layer in the native alumina for dense (c) or porous (d) systems. (e-f) snapshots highlighting the penetration level of Al initially belonging to the Al region (in violet) after the 700 K annealing, for the dense system (left) and the porous system (right).

Second, the direct contact between *am*Al_2O_3 and CuO in the dense system leads to the amorphization of the first layers of CuO, which becomes significant at 500 K. While CuO top layers remain in place, being well aligned in the (001) plane, roughly half of the top O layer is stripped off to build locally a novel Cu-O-Al-O arrangement (**Figure 2c** and **Figure 3e**). It is illustrated by the decrease of the average coordination number of Cu at increasing temperatures: from 3.96 at 400 K to 3.57 at 900 K. At the same time, in CuO, the average coordination number of Cu is 4 (supporting information file **Figure S3**). At 800 K, the changes observed lead to the formation of a thin ternary aluminate layer (~10 - 20 % of whole Al_xO_y region) made of a mixture of Al, O and Cu atoms, denoted as $Al_xO_yCu_z$ in **Figure 2c-d**. The ternary layer is characterized by the presence of Cu-Al bonds with an interatomic

distance of about 3.10 Å (**Figure 4a-b)**. The main mechanism responsible for the formation of this ternary aluminate region is the penetration of Al atoms originally belonging to the *am*Al_2O_3 into the first layers of CuO, thus creating, in addition to the Cu-Al discussed above, new Al_{AlxOy}-O_{CuO} bonds having an average bond length of 1.83 Å (**Figure 4d**). Its thickness increases with increasing temperature, from 2 nm at 500 K to 2.7 nm at 900 K, and is accompanied by an increase in the average coordination number of Cu with respect to Al (**Figure 4c**). No migration of atomic Cu from CuO to the new Al_xO_y region is observed, possibly explained by the fixation of Cu in the ternary oxide, and/or due to the crystalline zone that forms in the alumina in the immediate contact to the ternary zone. The crystalline zone is a few atomic layers thick, as clearly visible on **Figure 2d**. The penetration of Al ions into CuO and counter-diffusion of oxygen was also reported experimentally during the physical deposition of Al on CuO when an interfacial layer made of a mixture of Cu, O and Al was characterized.[50] In experiments, the formation of Al_2Cu phases was also observed (eutectic peak at 548 °C was clearly resolved in the DSC traces). However, intermetallics are not observed in the simulation, maybe due to insufficient simulation time.

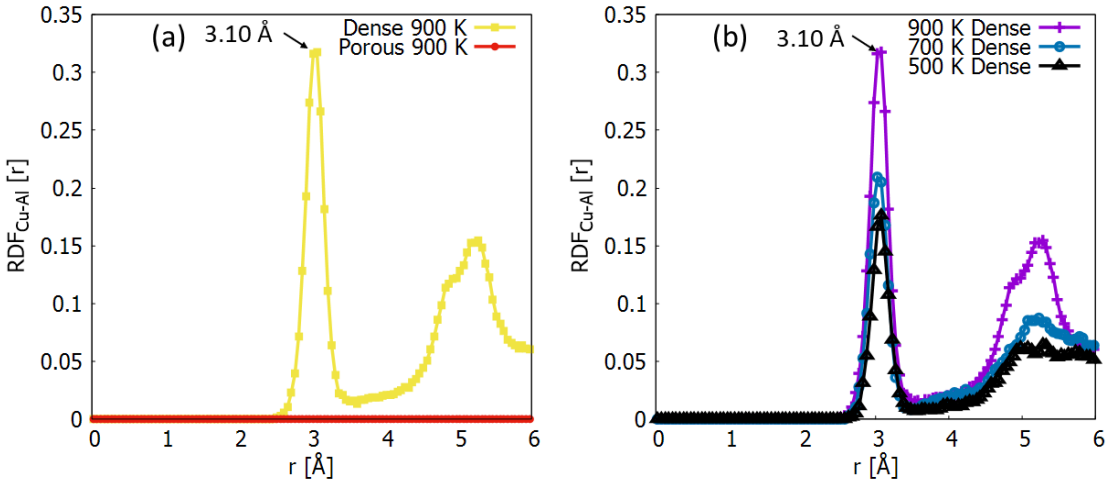

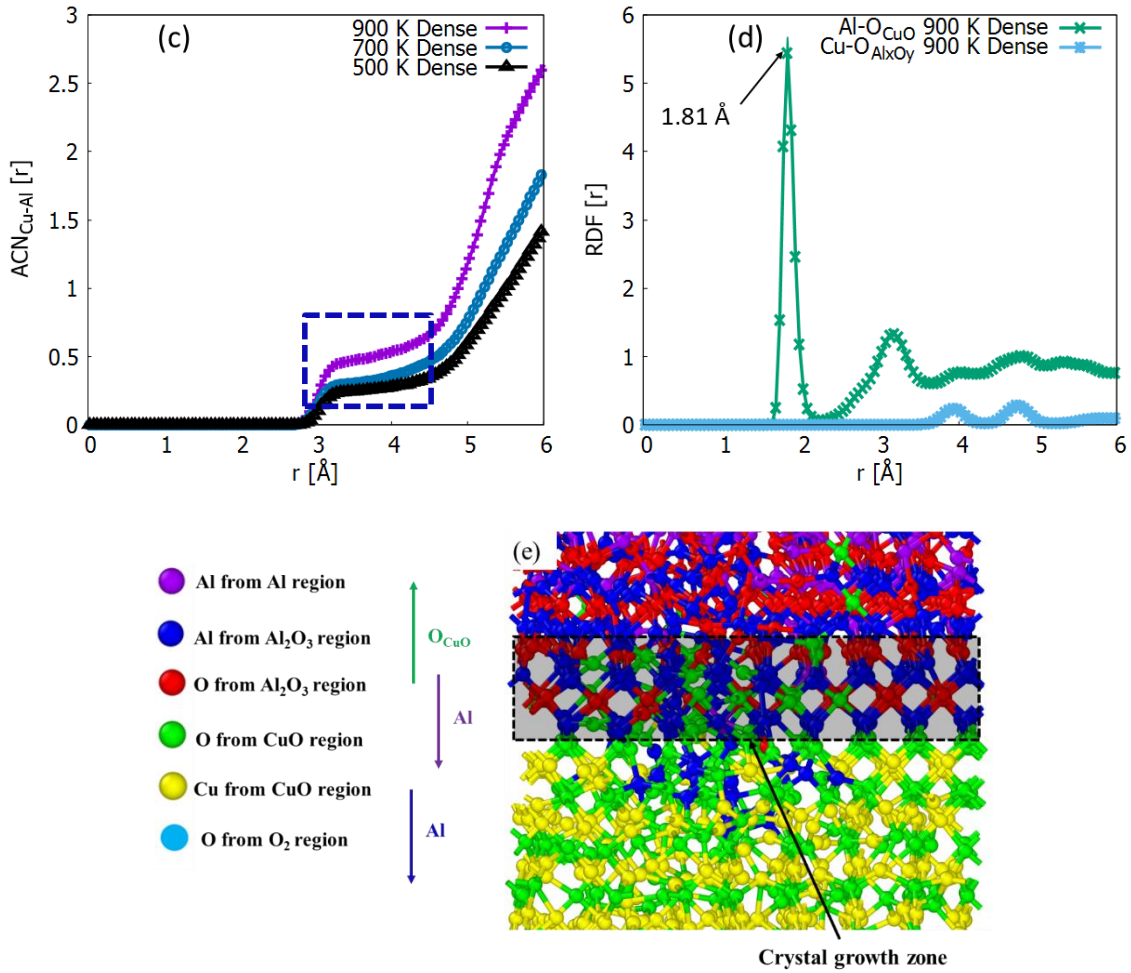

Figure 4. Aluminate interface characteristics: (a) Cu-Al radial distribution function (RDF) at the CuO-Al_xO_y interface for the dense (violet) and porous (green) system. (b-c) Cu-Al RDF and their accumulated function corresponding to the average coordination number (ACN) of Cu with respect to surrounding Al atoms at the CuO-Al_xO_y interface for the dense system at different annealing temperatures (500, 700 and 900 K). (d) Al-O_{CuO} and Cu-O_{AlxOy} RDF at the CuO-Al_xO_y interface. (e) snapshot of the CuO-Al_xO_y interface after annealing at 900 K – 5 ns. The green arrow represents the oxygens migration from the CuO to the Al_xO_y; the blue arrow represents the Al migration from the Al_xO_y to the CuO; and, the purple arrow represents the Al migration from the Al region to the Al_xO_y. RDF and ACN were calculated within the last 0.5 ns.

Overall, these first observations strongly suggest that the thin ternary aluminate layer, involving both Al and Cu slows down diffusion-driven reaction in the alumina layer for the fully-dense system. Lack of such ternary layer in porous composites may explain their experimentally observed enhanced reactivity compared to fully-dense composites. Next, the diffusion-driven reactions in the growing alumina upon annealing are quantified for both systems to better understand the impact of the thin ternary aluminate layer on the system reactivity.

3.2. Growth of an Al-rich Al_xO_y in place of the initial $amAl_2O_3$: porous vs dense.

One important finding of this theoretical study is the interfacial region enrichment with Al atoms from the Al region leading to the formation of an Al-rich layer in contact with either the pore or CuO surface. The number of Al atoms migrating from the Al region into the growing alumina layer is plotted in **Figure 5a** as a function of the annealing temperature for both dense and porous configurations. We note that the Al enrichment is systematically more pronounced in the porous system. After 5 ns at 400 K, the amount of additional Al represents 41% of the total Al species in Al_xO_y for the dense system while it reaches 45% for the porous system. At 900 K, the amount of additional Al in the Al_xO_y exceeds 50%: it represents 56 and 64% of the total Al species for the dense and porous system, respectively. Concomitantly to the Al enrichment, the interfacial region increases in thickness by growing into the Al region (**Figure 5b**). The atomic composition of the alumina region is quantified at different annealing temperatures and plotted in **Figure 5c** for the two systems: starting at 1.5 in the native (un-annealed) *am*Al_2O_3, the O/Al ratio drops down to ~0.9 after annealing at 400 K. Then, the O/Al atomic ratio decreases nearly linearly with the annealing temperature. For 800 K, the ratios become 0.58 and 0.72 for the porous and dense system, respectively. The observed trend confirms that Al enrichment is more pronounced in the porous system within

the temperature range considered. It has to be noted that the decrease in the O/Al ratio is also characterized by a decrease in the average coordination number of Al (**Figure 5d**).

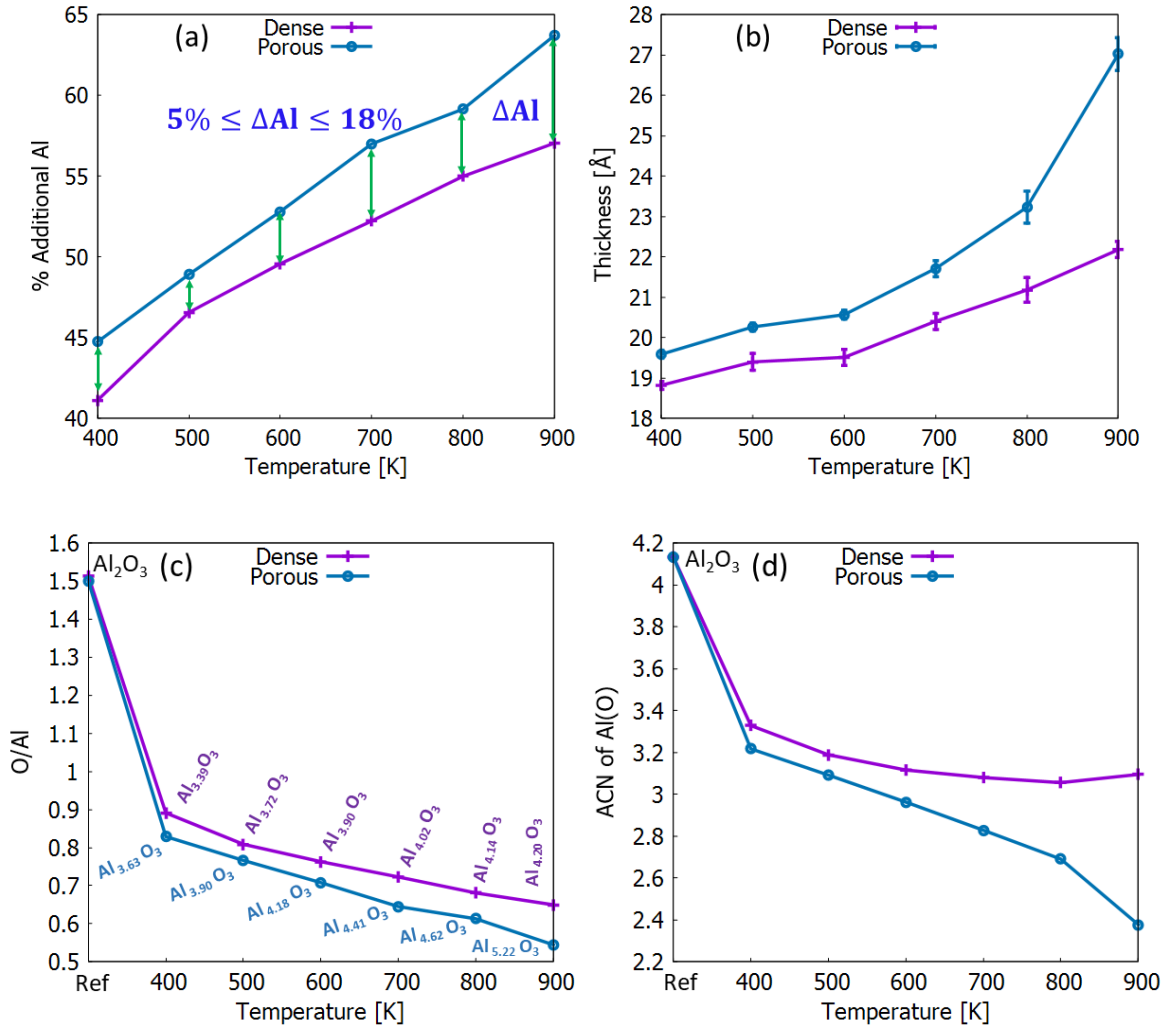

Figure 5. (a) Evolution of the amount of Al ions added in the Al_xO_y region in dense and porous systems as a function of the annealing temperatures. These values are computed as the average values over the last 0.5 ns of the simulation, where the variations of these quantities as a function of the simulation time reach their equilibrium (supporting information file **Figure S1a-b**). (b) Evolution of the thickness of the growing Al_xO_y region in dense and porous systems as a function of the annealing temperature. These values are computed as the average values over those of 10 structures over the last 100 ps. (c) O/Al ratio and (d) average coordination number (ACN) of Al with respect to O in the Al_xO_y

region for dense and porous systems, respectively. These values are computed as the average values over the last 0.5 ns where the variations of these quantities as a function of the simulation time reach their equilibrium (supporting information file **Figure S1c-f**). Stoichiometry of growing Al_xO_y interface is added for information.

The growth of the Al-rich Al_xO_y in place of the initial *am*Al_2O_3 barrier layer is a not only caused by the diffusion of aluminum ions towards the interface with either the pore or CuO, but also by the counter diffusion of oxygen atoms towards the pure aluminum, and their reactions. Indeed, the metallic Al ions, i.e., those initially belonging to the Al region, attract oxygen atoms from the deepest layer of the native *am*Al_2O_3 given the Coulomb long-range interaction established between both regions. The diffusion paths follows the free volume present in the aluminum oxide glassy state[45]. In the dense system, the oxygen atoms belonging to the deepest atomic layer of the native *am*Al_2O_3, i.e., those interfacing *am*Al_2O_3 and CuO, are also influenced by the CuO presence, which inhibits their participation in the creation of the reactive Al_xO_y compared to what is observed for the porous system. This is the main reason of the difference in the growth rate and composition of the Al_xO_y formed in porous and dense systems. Next, the spatial arrangements of Al ions in the Al_xO_y are analyzed in order to discriminate, which of the interface between those grown in porous or in dense system is the most reactive.

3.3. Al coordination in the growing Al_xO_y region: porous vs dense.

Aluminum 5-fold coordination (Al^V) coexisting with 4-and 6-fold coordination (Al^{IV}, Al^{VI}) structurally characterizes the amorphous alumina [51,52]. At 300 K, our *am*Al_2O_3 is characterized by an Al-O distance of 1.78 Å and contains 4% of Al^{III}, 77 % of Al^{IV} and 19% of Al^V (supporting information **Figure S4**). **Figure 6** gives the spatial distribution of the Al ions (Al^I, Al^{II}, Al^{III}, Al^{IV} and Al^V) in the Al_xO_y grown at different annealing temperatures. In

both systems, upon annealing, we observe a decrease in the number of Al^{V}, which disappears completely after annealing at 800 K. This is consistent with the continuous enrichment of Al_xO_y with Al as discussed in the previous section.

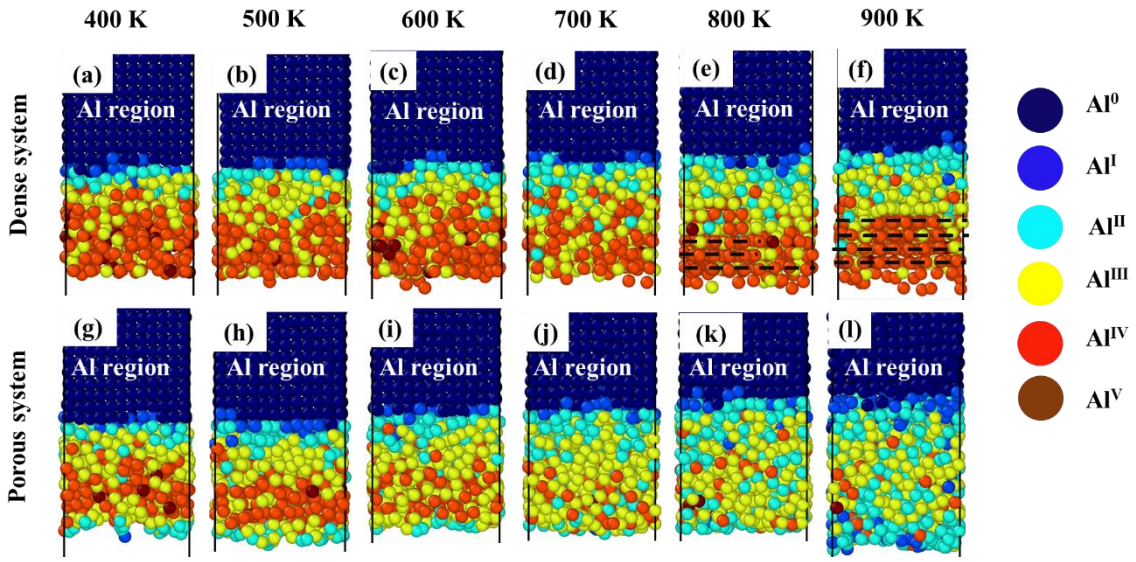

Figure 6. Snapshot after annealing process over 5 ns accompanied by the distribution of different types of Al ions in the Al_xO_y region at different temperatures where the top represents the dense system and the bottom represents the porous system. Images a, b, c, d, e, f correspond to dense system annealed at 400, 500, 600, 700, 800, and, 900 K, respectively. Images g, h, i, j, k, l correspond to porous system annealed at 400, 500, 600, 700, 800, and, 900 K respectively. The dotted lines shown in the image corresponding to the fully dense system at 800 K and 900 K indicate the initial growth of alumina crystals from the Al_xO_y region on CuO.

As a main observation, after annealing at 600 K, the spatial arrangement of the different Al ions (Al^{I}, Al^{II}, Al^{III} and Al^{IV}) in the Al_xO_y regions evolves differently for the two systems. In the dense system, the Al_xO_y interfacial layer includes three distinct zones:

i) near the Al-Al_xO_y interface, there is a region composed mainly of weakly-coordinated Al^{I} and Al^{II}, characterizing a highly reactive zone,

ii) a central region dominated by Al^{III},

iii) close to the Al_xO_y-CuO interface, there is a region showing an ordered arrangement of Al^{IV} ions (polyhedral), the highest coordinated Al ions, characterizing a zone with reduced reactivity.

By contrast, in porous system, the different Al ions are more uniformly dispersed in the entire Al_xO_y layer with a predominance of Al^{I} and Al^{II} at both Al-Al_xO_y and Al_xO_y–pore surfaces (**Figure 6d-e**). These two weak Al coordination regions are more responsive to oxygen compared to the central zone dominated by the Al^{III} ions.

The predominance of Al^{II} ions at the Al_xO_y–pore surface compared to predominance of Al^{IV} ions at the Al_xO_y–CuO interface might explain the low-temperature reactivity of Al/CuO thermite with nanopores. Indeed, the Al_xO_y–pore is almost totally depleted from its oxygen atoms with only Al^{III} , Al^{II} and Al^{I} ions present (**Figure 6a-c**). Accordingly, at 600 K, re-oxidation is observed (loss of Al^{II} and Al^{I}), due to chemisorption of the oxygens initially present in the form of O_2 molecules in the pore. This can explain the small exotherm at 600 K found on DSC traces of Al/CuO dense composites containing nanopores.[32] Importantly, the adsorption and reaction of the 13 O_2 molecules into the alumina layer at 700 K (12 O at 600 K and the remaining 14 O at 700 K) provokes a drop in the oxygen partial pressure in the pore which further prompts the CuO reduction into Cu_2O. The temperature-pressure region of formation of CuO, Cu_2O (supporting information file **Figure S6)** shows that below 10 mbar, CuO spontaneously decomposes into Cu_2O in the temperature range of 600 – 1000 K. [53,54] We can, therefore, conclude that CuO surface around the pore decomposes into Cu_2O and releases oxygen at temperatures greater than 600 K, which again corroborates the experimental observations of both gaseous oxygen at the interfaces [55] and Cu nanodots at the particle interfaces in porous systems recovered after heating to 650 K.

3.4. Increased surface reactivity in porous system.

Taking into consideration this last result, to further analyze the difference of reactivity between both systems we held them at 700 K for 5 ns, a temperature slightly lower than the common ignition temperatures seen in dense Al/CuO thermites, and considered the Al/Al_xO_y structure (i.e. preceding systems without the CuO slab or pore) exposed to an O_2 atmosphere (unlimited free O_2 molecules reservoir). Details are given in supporting information file **Figure S7**. At the end, the amount of oxygen consumed by Al/Al_xO_y of either the dense or the porous system, referred to as Al/$(Al_xO_{y)d}$ and Al/$(Al_xO_{y)p}$, is computed as a function of the annealing time. **Figure 7a** clearly shows that the Al/$(Al_xO_{y)p}$ consumes the oxygen molecules from the beginning of this simulation spontaneously when O_2 is in contact with the Al_xO_y surface. In contrast, the Al/$(Al_xO_{y)d}$ shows a delay about 60 ps for the structure to start consuming O_2 molecules (**Figure 7b**). Besides, the final number of oxygen atoms, consumed by Al/$(Al_xO_y)_p$ after 3 ns is nearly twice as large as that consumed by Al/$(Al_xO_y)_d$.

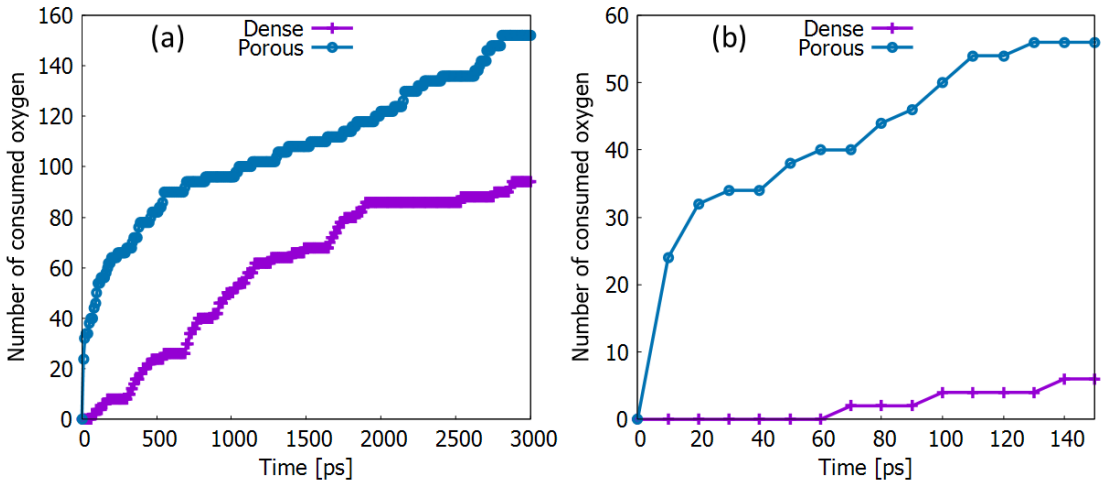

Figure 7. (a) amount of oxygen from gaseous O_2 consumed by the Al_xO_y-Al system over 3 ns at 700 K (b) zoom on the first 140 ps.

These results suggest that for the porous system, kinetics is limited by the oxidation reaction (initially spontaneous and exothermic) whereas for the dense system, it is clearly limited by diffusion.

Finally, the diffusion coefficients of both Al and O atoms through the differently grown Al_xO_y layers are calculated and compared with those of amorphous alumina (native glassy state) serving as the reference material. For that purpose, the mean square displacements (MSD) for Al and O in different aluminas were calculated and averaged to establish statistical significance[56]. After obtaining the average MSD for Al and O, the diffusion coefficients (D_O^{AlxOy} , D_{Al}^{AlxOy}) are determined as the slopes of the respective MSD curves[56]. **Figure 8** gives the results as logarithm of the diffusion coefficients**.** As expected, the Log diffusion coefficients of Al and O in the amorphous alumina (light blue data in **Figure 8a-b)** increase linearly with temperature from -17.82 (300 K) to -17.27 (900 K) and from -17.95 (300 K) to -17.28 (900 K), respectively. D_O^{Al2O3} *and* D_{Al}^{Al2O3} are of the same order of magnitude and the effect of temperature below 900 K is not significant. This observation is in good agreement with previous experimental studies on the diffusion of O and Al atoms in an alumina crystalline material. where Log (D) of Al (at 1540 K) and O (at 1550 K) are -13.40 and -14 respectively. [57,58]

The diffusion coefficients of Al and O in the Al_xO_y layers remain of the same order of magnitude as their diffusion coefficients in amorphous Al_2O_3 (see **Table 1**). However, the temperature effect on diffusion coefficients in the Al_xO_y layers depends on the presence of pores:

- in the dense system, both $\log(D_O^{AlxOy})$ and $\log(D_{Al}^{AlxOy})$ increase suddenly above 500 K; $\log(D_O^{AlxOy})$ increases from -17.7 to -16.6 and $\log(D_{Al}^{AlxOy})$ increases from -17.8 to -16.9.
- in the porous system, both $\log(D_O^{AlxOy})$ and $\log(D_{Al}^{AlxOy})$ increase suddenly above 500 K; $\log(D_O^{AlxOy})$ increases from -17.5 to -17.0 and $\log(D_{Al}^{AlxOy})$ increases from -17.8 to -17.0.

This confirms that the presence of pores activates the diffusion of O through the Al_xO_y layer at a lower temperature (~600 K against 800 K w/o pore). It has to be noted that Al and O diffuse at comparable rates in the porous systems, whereas Al diffuses faster than O in the dense system.

Table 1. Diffusion of oxygen and aluminum in amorphous material of pristine alumina and interfacial alumina in porous and dense systems.

Temperature (K)	Diffusion coefficient -Log (D) ($cm^2.s^{-1}$)					
	Amorphous Al_2O_3		Al-rich Al_xO_y			
			porous system		dense system	
	Oxygen	Aluminum	Oxygen	Aluminum	Oxygen	Aluminum
300	17.58	17.80	17.58	17.8	17.82	17.95
500	17.57	17.80	17.50	17.79	17.57	17.7
700	17.74	17.79	16.97	16.98	17.42	17.44
900	16.57	16.91	16.87	16.84	17.27	17.28

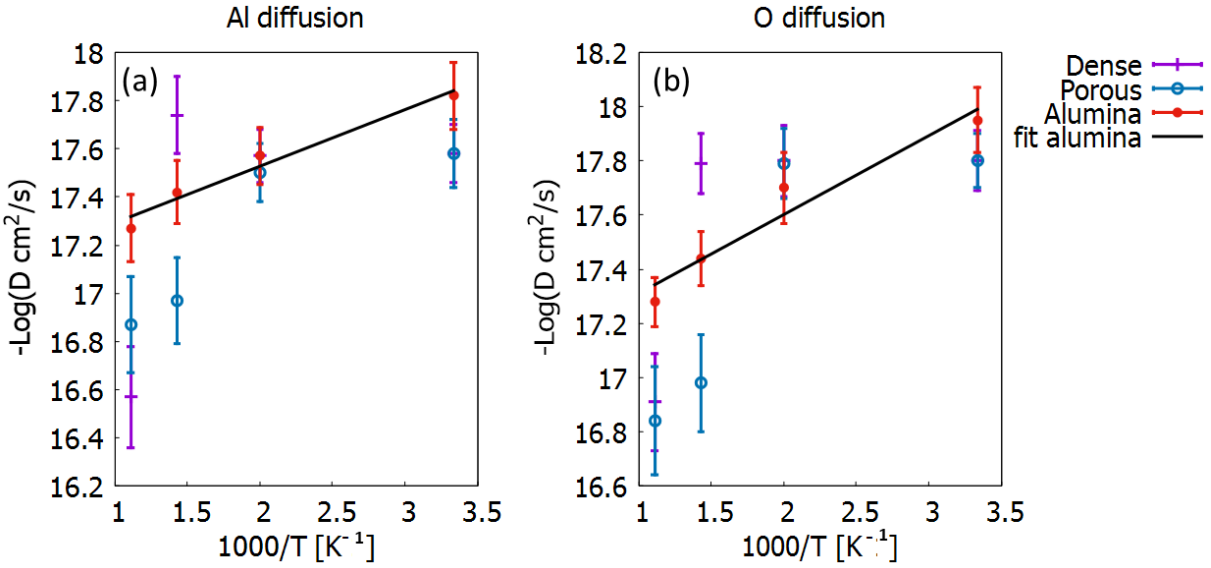

Figure 8. Log diffusion coefficients as a function of reciprocal temperature for Al (a) and O (b) in *am*Al_2O_3, and the different Al_xO_y regions grown upon annealing in the porous and dense system. The average MSD is computed in the last nanosecond of our trajectory at each temperature (supporting information file **Figure S5**).

4. Conclusions

This theoretical work investigated the influence of pores at the CuO-Al interfaces on the pre-ignition reaction processes using ReaxFF molecular dynamics simulations. The chemical and structural evolution of the reacting interface between the Al and CuO layers upon annealing up to 900 K were studied at the atomic scale, considering two interfacial structures: with and without a pore (1 nm spacing between Al and CuO surfaces, containing 13 O_2 molecules). One major finding of this theoretical study is that in both, porous and dense systems there is a growing Al_2O_{3-y} interface layer continuously enriched with Al ions from the Al fuel reservoir, replacing the initial amorphous alumina barrier layer. However, this evolution towards a more reactive interfacial layer occurs differently for the dense and porous composites at temperatures above 600 K. First, the direct contact between *am*Al_2O_3 and CuO leads to the formation of a thin ternary copper aluminate phase (comprising ~10 - 20 % of the whole Al_xO_y layer at 800 K) made of a mixture of Al, O and Cu atoms. This ternary phase impedes further growth of the Al_xO_y layer and thus reduces the nanothermite reactivity, evaluated in this study in terms of the diffusion coefficients for both O and Al. Instead, the presence of a pore between the *am*Al_2O_3 and CuO activates the dissociative adsorption of the gaseous O_2 molecules from the pore onto the alumina surface at temperatures of 600 K and above. This leads to massive depletion of oxygen available near the alumina surface (recognizable as a predominance of Al^{II} ions at the pore surface compared to predominance of Al^{IV} ions at the Al–CuO interface in dense system) rendering the interfacial Al_xO_y layer highly reactive at 600

K and above. In addition, the O_2 pressure drop in the pore is expected to accelerate reduction of adjacent CuO surface. These findings can thus explain the presence of copper nanodots and decrease in the ignition temperature observed experimentally for layered or milled Al/CuO composites containing nanopores.

Associated content

Supporting Information

The Supporting Information is available free of charge on the ACS Publications website at DOI:

Further analysis of the ReaxFF dynamic simulations:

- The temporal evolution of the quantity characterizes the nanothermite Al/CuO interface for dense and porous systems such as the total number of Al in the Al_xO_y interfacial region, the average coordination number (ACN) of Al with respect to oxygen and the O/Al ratio.
- Different oxidation states of Al in the Al_xO_y interfacial region for dense and porous systems as a function of temperature.
- Initial structure for the study of Al_xO_y-Al surface reactivity resulting from the annealing of dense and porous systems at 700 K.
- The temperature-pressure region of formation of CuO, Cu_2O, Cu

Authors information

Corresponding Author

Carole Rossi – LAAS-CNRS, University of Toulouse, 31077 Toulouse, France; orcid.org/0000-0003-3864-7574; E-mail: rossi@laas.fr

Authors

Hicham Jabraoui– LAAS-CNRS, University of Toulouse, 31077 Toulouse, France; orcid/org/0000-0003-1201-8358

Mirko Schoenitz − New Jersey Institute of Technology, Newark, New Jersey 07103, United States; orcid.org/0000-0002-9142-8162

Alain Esteve – LAAS-CNRS, University of Toulouse, 31077 Toulouse, France; orcid.org/0000-0002-0301-7479

Edward L. Dreizin − New Jersey Institute of Technology, Newark, New Jersey 07103, United States; orcid.org/ 0000-0003-0859-0984

Author contributions

All authors contributed equally in this work.

Funding sources

C.R. received funding from the European Research Council (ERC) under the European Union's Horizon 2020 research and innovation program (grand agreement No. 832889 - pyrosafe).

Competing financial interests

The authors declare no competing financial interests.

Acknowledgements

The authors grateful acknowledge support from the European Research Council (H2020 Excellent Science) Researcher Award (grant 832889 – PyroSafe). This work was performed using high power computing resources from CALMIP.

References

(1) Umbrajkar, S. M.; Schoenitz, M.; Dreizin, E. L. Exothermic Reactions in Al–CuO Nanocomposites. *Thermochimica Acta* **2006**, *451* (1), 34–43. https://doi.org/10.1016/j.tca.2006.09.002.

(2) Fischer, S.; Grubelich, M. A Survey of Combustible Metals, Thermites, and Intermetallics for Pyrotechnic Applications. In *32nd Joint Propulsion Conference and Exhibit*; American Institute of Aeronautics and Astronautics. https://doi.org/10.2514/6.1996-3018.

(3) Rossi, C. Engineering of Al/CuO Reactive Multilayer Thin Films for Tunable Initiation and Actuation. *Propellants, Explosives, Pyrotechnics* **2019**, *44* (1), 94–108. https://doi.org/10.1002/prep.201800045.
(4) Xu, F.; Biswas, P.; Nava, G.; Schwan, J.; Kline, D. J.; Rehwoldt, M. C.; Mangolini, L.; Zachariah, M. R. Tuning the Reactivity and Energy Release Rate of I2O5 Based Ternary Thermite Systems. *Combustion and Flame* **2021**, *228*, 210–217. https://doi.org/10.1016/j.combustflame.2020.12.047.
(5) Dombroski, D. M. B.; Wang, A.; Wen, J. Z.; Alfano, M. Joining and Welding with a Nanothermite and Exothermic Bonding Using Reactive Multi-Nanolayers – A Review. *Journal of Manufacturing Processes* **2022**, *75*, 280–300. https://doi.org/10.1016/j.jmapro.2021.12.056.
(6) Koch, E.-C.; Knapp, S. Thermites – Versatile Materials. *Propellants, Explosives, Pyrotechnics* **2019**, *44* (1), 7–7. https://doi.org/10.1002/prep.201980131.
(7) Liu, X.; Schoenitz, M.; Dreizin, E. L. Preparation, Ignition, and Combustion of Magnesium-Calcium Iodate Reactive Nano-Composite Powders. *Chemical Engineering Journal* **2019**, *359*, 955–962. https://doi.org/10.1016/j.cej.2018.11.091.
(8) Nakpan, W.; Grinshpun, S. A.; Yermakov, M.; Indugula, R.; Reponen, T.; Wang, S.; Schoenitz, M.; Dreizin, E. L. Inactivation of Aerosolized Surrogates of Bacillus Anthracis Spores by Combustion Products of Aluminum- and Magnesium-Based Reactive Materials: Effect of Exposure Time. *Aerosol Science and Technology* **2018**, *52* (5), 579–587. https://doi.org/10.1080/02786826.2018.1432028.
(9) Glavier, L.; Nicollet, A.; Jouot, F.; Martin, B.; Barberon, J.; Renaud, L.; Rossi, C. Nanothermite/RDX-Based Miniature Device for Impact Ignition of High Explosives. *Propellants, Explosives, Pyrotechnics* **2017**, *42* (3), 308–317. https://doi.org/10.1002/prep.201600154.
(10) Fu, S.; Shen, R.; Zhu, P.; Ye, Y. Metal–Interlayer–Metal Structured Initiator Containing Al/CuO Reactive Multilayer Films That Exhibits Improved Ignition Properties. *Sensors and Actuators A: Physical* **2019**, *292*, 198–204. https://doi.org/10.1016/j.sna.2019.04.019.
(11) Salvagnac, L.; Assie-Souleille, S.; Rossi, C. Layered Al/CuO Thin Films for Tunable Ignition and Actuations. *Nanomaterials* **2020**, *10* (10), 2009. https://doi.org/10.3390/nano10102009.
(12) Rodríguez, G. A. A.; Suhard, S.; Rossi, C.; Estève, D.; Fau, P.; Sabo-Etienne, S.; Mingotaud, A. F.; Mauzac, M.; Chaudret, B. A Microactuator Based on the Decomposition of an Energetic Material for Disposable Lab-on-Chip Applications: Fabrication and Test. *J. Micromech. Microeng.* **2008**, *19* (1), 015006. https://doi.org/10.1088/0960-1317/19/1/015006.
(13) Nicollet, A.; Salvagnac, L.; Baijot, V.; Estève, A.; Rossi, C. Fast Circuit Breaker Based on Integration of Al/CuO Nanothermites. *Sensors and Actuators A: Physical* **2018**, *273*, 249–255. https://doi.org/10.1016/j.sna.2018.02.044.
(14) Apperson, S. J.; Bezmelnitsyn, A. V.; Thiruvengadathan, R.; Gangopadhyay, K.; Gangopadhyay, S.; Balas, W. A.; Anderson, P. E.; Nicolich, S. M. Characterization of Nanothermite Material for Solid-Fuel Microthruster Applications. *Journal of Propulsion and Power* **2009**, *25* (5), 1086–1091. https://doi.org/10.2514/1.43206.
(15) Zhu, P.; Hou, G.; Wang, H.; Xu, C.; Zhao, S.; Shen, R. Design, Preparation, and Performance of a Planar Ignitor Inserted With PyroMEMS Safe and Arm Device. *Journal of Microelectromechanical Systems* **2018**, *27* (6), 1186–1192. https://doi.org/10.1109/JMEMS.2018.2875707.
(16) Rossi, C. Nano-Engineering of Al/CuO Multilayers: Bridging the Gap Between Research and Applications. In *Energetic Materials Gordon Research Conference*; Newry, United States, 2018; p 2p.
(17) Bahrami, M.; Taton, G.; Conédéra, V.; Salvagnac, L.; Tenailleau, C.; Alphonse, P.; Rossi, C. Magnetron Sputtered Al-CuO Nanolaminates: Effect of Stoichiometry and Layers Thickness on Energy Release and Burning Rate. *Propellants, Explosives, Pyrotechnics* **2014**, *39* (3), 365–373. https://doi.org/10.1002/prep.201300080.

(18) Wang, H.; Julien, B.; Kline, D. J.; Alibay, Z.; Rehwoldt, M. C.; Rossi, C.; Zachariah, M. R. Probing the Reaction Zone of Nanolaminates at ∼μs Time and ∼μm Spatial Resolution. *J. Phys. Chem. C* **2020**, *124* (25), 13679–13687. https://doi.org/10.1021/acs.jpcc.0c01647.
(19) Schoenitz, M.; Ward, T. S.; Dreizin, E. L. Fully Dense Nano-Composite Energetic Powders Prepared by Arrested Reactive Milling. *Proceedings of the Combustion Institute* **2005**, *30* (2), 2071–2078. https://doi.org/10.1016/j.proci.2004.08.134.
(20) Dai, J.; Wang, C.; Wang, Y.; Xu, W.; Xu, J.; Shen, Y.; Zhang, W.; Ye, Y.; Shen, R. From Nanoparticles to On-Chip 3D Nanothermite: Electrospray Deposition of Reactive Al/CuO@NC onto Semiconductor Bridge and Its Application for Rapid Ignition. *Nanotechnology* **2020**, *31* (19), 195712. https://doi.org/10.1088/1361-6528/ab6fd8.
(21) Wang, Y.; Zhang, X.; Xu, J.; Shen, Y.; Wang, C.; Li, F.; Zhang, Z.; Chen, J.; Ye, Y.; Shen, R. Fabrication and Characterization of Al–CuO Nanocomposites Prepared by Sol-Gel Method. *Defence Technology* **2021**, *17* (4), 1307–1312. https://doi.org/10.1016/j.dt.2020.06.029.
(22) Palussière, S.; Cure, J.; Nicollet, A.; Fau, P.; Fajerwerg, K.; L. Kahn, M.; Estève, A.; Rossi, C. The Role of Alkylamine in the Stabilization of CuO Nanoparticles as a Determinant of the Al/CuO Redox Reaction. *Physical Chemistry Chemical Physics* **2019**, *21* (29), 16180–16189. https://doi.org/10.1039/C9CP02220A.
(23) Calais, T.; Bourrier, D.; Bancaud, A.; Chabal, Y.; Estève, A.; Rossi, C. DNA Grafting and Arrangement on Oxide Surfaces for Self-Assembly of Al and CuO Nanoparticles. *Langmuir* **2017**, *33* (43), 12193–12203. https://doi.org/10.1021/acs.langmuir.7b02159.
(24) Shende, R.; Subramanian, S.; Hasan, S.; Apperson, S.; Thiruvengadathan, R.; Gangopadhyay, K.; Gangopadhyay, S.; Redner, P.; Kapoor, D.; Nicolich, S.; Balas, W. Nanoenergetic Composites of CuO Nanorods, Nanowires, and Al-Nanoparticles. *Propellants, Explosives, Pyrotechnics* **2008**, *33* (2), 122–130. https://doi.org/10.1002/prep.200800212.
(25) Malchi, J. Y.; Foley, T. J.; Yetter, R. A. Electrostatically Self-Assembled Nanocomposite Reactive Microspheres. *ACS Appl. Mater. Interfaces* **2009**, *1* (11), 2420–2423. https://doi.org/10.1021/am900521w.
(26) Stamatis, D.; Ermoline, A.; Dreizin, E. L. A Multi-Step Reaction Model for Ignition of Fully-Dense Al-CuO Nanocomposite Powders. *Combustion Theory and Modelling* **2012**, *16* (6), 1011–1028. https://doi.org/10.1080/13647830.2012.694480.
(27) Lanthony, C.; Ducéré, J.-M.; Estève, A.; Rossi, C.; Djafari-Rouhani, M. Formation of Al/CuO Bilayer Films: Basic Mechanisms through Density Functional Theory Calculations. *Thin Solid Films* **2012**, *520* (14), 4768–4771. https://doi.org/10.1016/j.tsf.2011.10.184.
(28) Xiong, G.; Yang, C.; Zhu, W. Interface Reaction Processes and Reactive Properties of Al/CuO Nanothermite: An Ab Initio Molecular Dynamics Simulation. *Applied Surface Science* **2018**, *459*, 835–844. https://doi.org/10.1016/j.apsusc.2018.08.069.
(29) Tang, C.-M.; Chen, X.-X.; Cheng, X.-L.; Zhang, C.-Y.; Lu, Z.-P. Ab Initio Molecular Dynamics Study of Thermite Reaction at Al and CuO Nano-Interfaces at Different Temperatures. *Chemical Physics Letters* **2018**, *699*, 171–181. https://doi.org/10.1016/j.cplett.2018.03.047.
(30) Petrantoni, M.; Rossi, C.; Salvagnac, L.; Conédéra, V.; Estève, A.; Tenailleau, C.; Alphonse, P.; Chabal, Y. J. Multilayered Al/CuO Thermite Formation by Reactive Magnetron Sputtering: Nano versus Micro. *Journal of Applied Physics* **2010**, *108* (8), 084323. https://doi.org/10.1063/1.3498821.
(31) Mily, E. J.; Oni, A.; LeBeau, J. M.; Liu, Y.; Brown-Shaklee, H. J.; Ihlefeld, J. F.; Maria, J.-P. The Role of Terminal Oxide Structure and Properties in Nanothermite Reactions. *Thin Solid Films* **2014**, *562*, 405–410. https://doi.org/10.1016/j.tsf.2014.05.005.
(32) Mursalat, M.; Huang, C.; Julien, B.; Schoenitz, M.; Esteve, A.; Rossi, C.; Dreizin, E. L. Low-Temperature Exothermic Reactions in Al/CuO Nanothermites Producing Copper Nanodots and Accelerating Combustion. *ACS Appl. Nano Mater.* **2021**, *4* (4), 3811–3820. https://doi.org/10.1021/acsanm.1c00236.

(33) Julien, B.; Cure, J.; Salvagnac, L.; Josse, C.; Esteve, A.; Rossi, C. Integration of Gold Nanoparticles to Modulate the Ignitability of Nanothermite Films. *ACS Appl. Nano Mater.* **2020**, *3* (3), 2562–2572. https://doi.org/10.1021/acsanm.9b02619.
(34) Wu, T.; Julien, B.; Wang, H.; Pelloquin, S.; Esteve, A.; Zachariah, M. R.; Rossi, C. Engineered Porosity-Induced Burn Rate Enhancement in Dense Al/CuO Nanothermites. *ACS Appl. Energy Mater.* **2022**. https://doi.org/10.1021/acsaem.1c03805.
(35) Egan, G. C.; Mily, E. J.; Maria, J.-P.; Zachariah, M. R. Probing the Reaction Dynamics of Thermite Nanolaminates. *J. Phys. Chem. C* **2015**, *119* (35), 20401–20408. https://doi.org/10.1021/acs.jpcc.5b04117.
(36) Jeon, B.; Sankaranarayanan, S. K. R. S.; van Duin, A. C. T.; Ramanathan, S. Reactive Molecular Dynamics Study of Chloride Ion Interaction with Copper Oxide Surfaces in Aqueous Media. *ACS Appl. Mater. Interfaces* **2012**, *4* (3), 1225–1232. https://doi.org/10.1021/am201345v.
(37) Sengul, M. Y.; Randall, C. A.; van Duin, A. C. T. ReaxFF Molecular Dynamics Study on the Influence of Temperature on Adsorption, Desorption, and Decomposition at the Acetic Acid/Water/ZnO(10$\bar{1}$0) Interface Enabling Cold Sintering. *ACS Appl. Mater. Interfaces* **2018**, *10* (43), 37717–37724. https://doi.org/10.1021/acsami.8b13630.
(38) J. Marsden, A.; Skilbeck, M.; Healey, M.; R. Thomas, H.; Walker, M.; S. Edwards, R.; A. Garcia, N.; Vuković, F.; Jabraoui, H.; R. Walsh, T.; P. Rourke, J.; R. Wilson, N. From Graphene to Graphene Oxide: The Importance of Extended Topological Defects. *Physical Chemistry Chemical Physics* **2022**, *24* (4), 2318–2331. https://doi.org/10.1039/D1CP04316A.
(39) Lanthony, C.; Guiltat, M.; Ducéré, J. M.; Verdier, A.; Hémeryck, A.; Djafari-Rouhani, M.; Rossi, C.; Chabal, Y. J.; Estève, A. Elementary Surface Chemistry during CuO/Al Nanolaminate-Thermite Synthesis: Copper and Oxygen Deposition on Aluminum (111) Surfaces. *ACS Appl. Mater. Interfaces* **2014**, *6* (17), 15086–15097. https://doi.org/10.1021/am503126k.
(40) Plimpton, S. Fast Parallel Algorithms for Short-Range Molecular Dynamics. *Journal of Computational Physics* **1995**, *117* (1), 1–19. https://doi.org/10.1006/jcph.1995.1039.
(41) Psofogiannakis, G. M.; McCleerey, J. F.; Jaramillo, E.; van Duin, A. C. T. ReaxFF Reactive Molecular Dynamics Simulation of the Hydration of Cu-SSZ-13 Zeolite and the Formation of Cu Dimers. *J. Phys. Chem. C* **2015**, *119* (12), 6678–6686. https://doi.org/10.1021/acs.jpcc.5b00699.
(42) Cao, H.; Zhou, Z.; Yu, J.; Zhou, X. DFT Study on Structural, Electronic, and Optical Properties of Cubic and Monoclinic CuO. *J Comput Electron* **2018**, *17* (1), 21–28. https://doi.org/10.1007/s10825-017-1057-9.
(43) Shimizu, K.; Furneaux, R. C.; Thompson, G. E.; Wood, G. C.; Gotoh, A.; Kobayashi, K. On the Nature of "Easy Paths" for the Diffusion of Oxygen in Thermal Oxide Films on Aluminum. *Oxid Met* **1991**, *35* (5), 427–439. https://doi.org/10.1007/BF00664713.
(44) Bouhadja, M.; Jakse, N.; Pasturel, A. Structural and Dynamic Properties of Calcium Aluminosilicate Melts: A Molecular Dynamics Study. *J. Chem. Phys.* **2013**, *138* (22), 224510. https://doi.org/10.1063/1.4809523.
(45) Jabraoui, H.; Charpentier, T.; Gin, S.; Delaye, J.-M.; Pollet, R. Atomic Insights into the Events Governing the Borosilicate Glass–Water Interface. *J. Phys. Chem. C* **2021**, *125* (14), 7919–7931. https://doi.org/10.1021/acs.jpcc.1c00388.
(46) Jabraoui, H.; Malki, M.; Hasnaoui, A.; Badawi, M.; Ouaskit, S.; Lebègue, S.; Vaills, Y. Thermodynamic and Structural Properties of Binary Calcium Silicate Glasses: Insights from Molecular Dynamics. *Phys. Chem. Chem. Phys.* **2017**, *19* (29), 19083–19093. https://doi.org/10.1039/C7CP03397D.
(47) Jabraoui, H.; Badawi, M.; Lebègue, S.; Vaills, Y. Elastic and Structural Properties of Low Silica Calcium Aluminosilicate Glasses from Molecular Dynamics Simulations. *Journal of Non-Crystalline Solids* **2018**, *499*, 142–152. https://doi.org/10.1016/j.jnoncrysol.2018.07.004.
(48) Jabraoui, H.; Achhal, E. M.; Hasnaoui, A.; Garden, J.-L.; Vaills, Y.; Ouaskit, S. Molecular Dynamics Simulation of Thermodynamic and Structural Properties of Silicate Glass: Effect of

the Alkali Oxide Modifiers. *Journal of Non-Crystalline Solids* **2016**, *448*, 16–26. https://doi.org/10.1016/j.jnoncrysol.2016.06.030.
(49) Jabraoui, H.; Vaills, Y.; Hasnaoui, A.; Badawi, M.; Ouaskit, S. Effect of Sodium Oxide Modifier on Structural and Elastic Properties of Silicate Glass. *J. Phys. Chem. B* **2016**, *120* (51), 13193–13205. https://doi.org/10.1021/acs.jpcb.6b09664.
(50) Kwon, J.; Ducéré, J. M.; Alphonse, P.; Bahrami, M.; Petrantoni, M.; Veyan, J.-F.; Tenailleau, C.; Estève, A.; Rossi, C.; Chabal, Y. J. Interfacial Chemistry in Al/CuO Reactive Nanomaterial and Its Role in Exothermic Reaction. *ACS Appl. Mater. Interfaces* **2013**, *5* (3), 605–613. https://doi.org/10.1021/am3019405.
(51) Landron, C.; Hennet, L.; Jenkins, T. E.; Greaves, G. N.; Coutures, J. P.; Soper, A. K. Liquid Alumina: Detailed Atomic Coordination Determined from Neutron Diffraction Data Using Empirical Potential Structure Refinement. *Phys. Rev. Lett.* **2001**, *86* (21), 4839–4842. https://doi.org/10.1103/PhysRevLett.86.4839.
(52) Glorieux, B.; Millot, F.; Rifflet, J.-C.; Coutures, J.-P. Density of Superheated and Undercooled Liquid Alumina by a Contactless Method. *International Journal of Thermophysics* **1999**, *20* (4), 1085–1094. https://doi.org/10.1023/A:1022650703233.
(53) Zhu, Y.; Mimura, K.; Isshiki, M. Oxidation Mechanism of Cu2O to CuO at 600–1050°C. *Oxidation of Metals* **2004**, *62* (3), 207–222. https://doi.org/10.1007/s11085-004-7808-6.
(54) Honjo, G. Electron Diffraction Studies on Oxide Films Formed on Metals and Alloys Part 1. Oxidation of Pure Copper. *J. Phys. Soc. Jpn.* **1949**, *4* (4–6), 330–333. https://doi.org/10.1143/JPSJ.4.330.
(55) Abdallah, I.; Zapata, J.; Lahiner, G.; Warot-Fonrose, B.; Cure, J.; Chabal, Y.; Esteve, A.; Rossi, C. Structure and Chemical Characterization at the Atomic Level of Reactions in Al/CuO Multilayers. *ACS Appl. Energy Mater.* **2018**, *1* (4), 1762–1770. https://doi.org/10.1021/acsaem.8b00296.
(56) Jabraoui, H.; Gin, S.; Charpentier, T.; Pollet, R.; Delaye, J.-M. Leaching and Reactivity at the Sodium Aluminosilicate Glass–Water Interface: Insights from a ReaxFF Molecular Dynamics Study. *J. Phys. Chem. C* **2021**. https://doi.org/10.1021/acs.jpcc.1c07266.
(57) Gall, M. L.; Lesage, B.; Bernardini, J. Self-Diffusion in α-Al2O3 I. Aluminium Diffusion in Single Crystals. *Philosophical Magazine A* **1994**, *70* (5), 761–773. https://doi.org/10.1080/01418619408242929.
(58) Prot, D.; Monty, C. Self-Diffusion in A–Al2O3. II. Oxygen Diffusion in 'Undoped' Single Crystals. *Philosophical Magazine A* **1996**, *73* (4), 899–917. https://doi.org/10.1080/01418619608243695.

TOC